Journal of Magnetism and Magnetic Materials 562 (2022) 169759

Contents lists available at ScienceDirect

Journal of Magnetism and Magnetic Materials

journal homepage: www.elsevier.com/locate/jmmm

Efficient spin–orbit torque magnetization switching by reducing domain nucleation energy

ARTICLE INFO

Keywords
Spin-orbit torque
Domain wall
Domain nucleation
Domain propagation
Switching energy

ABSTRACT

Spin-orbit torque (SOT) induced magnetization switching occurs via either coherent switching for devices with sizes comparable to a single domain, or domain nucleation followed by domain wall (DW) propagation for the larger devices. This study reveals that the energy required in domain nucleation is up to five times higher than DW propagation to achieve magnetization switching for any device smaller than 100 nm. Hence, the minimization of the domain nucleation energy is critical to the optimization of energy efficiency. The reduction in domain nucleation energy is demonstrated in this work using an external magnetic field and the Dzyaloshinskii–Moriya interaction. Lastly, to capitalize on the energy difference between domain nucleation and DW propagation, we propose a two-pulse scheme that utilizes a brief high-power pulse to initiate domain nucleation followed by a longer low-power pulse for DW propagation. The two-pulse scheme can achieve energy savings of up to 72 % compared to using a single-pulse scheme. Our result determines that the two-pulse scheme has strong potential for significant improvements in SOT switching energy efficiency.

1. Introduction

Memory devices are now an integral part of our daily lives with the advent of artificial intelligence (AI), 5G communication technology and the Internet of Things (IoT) [1,2]. Magnetoresistive random-access memory (MRAM) is one promising non-volatile memory system with high scalability and speed [3,4]. Moreover, it is also attractive in nonconventional computing, such as in-memory computing, neuromorphic computing due to its low power consumption [5]. Progressing beyond magnetic field-written MRAM, electrical current-based writing schemes currently take centre stage for their high speed and energy efficiency through either spin-transfer torque (STT) or spin–orbit torque (SOT) [6,7]. In the STT writing scheme, electrical currents are injected perpendicular to the memory cell to induce spin-polarization via interaction with the magnetic reference layer. The spin angular momentum from the spin-polarized current is transferred to the ferromagnetic memory layer's magnetization, switching the magnetization direction under sufficient torque exerted by the spin-polarized current [8]. The high current density required does not only cost significant energy but also exerts unwanted electrical stress on the insulating barrier of the magnetic tunnel junction (MTJ), which drastically limits its endurance [9,10,11,12]. The newer SOT-MRAM emerged as an alternative electrical current-based writing scheme where the writing current does not flow across the MTJ barrier. In the SOT-MRAM scheme, the spin Hall effect (SHE) and Rashba–Edelstein effect dominate the conversion of the charge current into spin current when an in-plane current flows through a heavy material layer [13,14,15]. Heavy metals like W [16], Ta [7,17], and Pt [18] with strong spin–orbit coupling breaks spin accumulation symmetry, leading to the generation of spin currents that flow transverse to the charge current. A ferromagnetic memory layer adjacent to these heavy metals then experiences SOT due to this spin current and potentially undergoes magnetization switching. In the dimensional limit of a single-domain MRAM, SOT-induced magnetization switching occurs via coherent switching. For larger devices beyond this limit, the switching occurs via domain nucleation followed by domain wall (DW) propagation [14,17,19,20,21]. To achieve high energy efficient SOT-MRAM, the domain nucleation energy reduction remains the primary direction. In addition, another promising approach is to optimize the current density applied for nucleating domain and DW propagation [22], such as using He^{+} ion irradiation to reduce DW nucleation energy [23], implementing STT to assist SOT switching [24,25]. In most works, single-pulsed currents are applied to perform magnetization switching, necessitating a high current density to nucleate a reversed domain, even though it is excessive for DW propagation [20,26]. Therefore, an opportunity lies in further optimizing the energy consumption of SOT-induced magnetization switching by addressing the discrepancy in current density requirements between domain nucleation and propagation. In this work, we first investigate the lowering of domain nucleation energy with an in-plane magnetic field and Dzyaloshinskii-Moriya interaction (DMI). Next, we study the two-pulse writing scheme with distinct current densities applied for domain nucleation and DW propagation. From this study, we demonstrate the significant switching energy reduction using the two-pulse writing scheme compared to that of the single-pulse current scheme. Taking the benefits of the low energy consumption in the two-pulse current scheme, it is not only significant for MRAM application, but also for DW-based racetrack memory, logic device, and MTJ [27,28,29].

2. Micromagnetic simulation parameters and structures

The numerical investigation in this work was performed by using Mumax3 [30]. We considered a general perpendicular magnetic anisotropy (PMA) heterostructure, comprising a CoFeB magnetic thin film, a MgO capping layer, and a W heavy metal seed layer, as illustrated in Fig. 1(a). The material parameters used were adopted from experimentally reported W/CoFeB/MgO [31,32,33,34,35]: the saturation

https://doi.org/10.1016/j.jmmm.2022.169759
Received 30 March 2022; Received in revised form 29 June 2022; Accepted 24 July 2022
Available online 6 August 2022

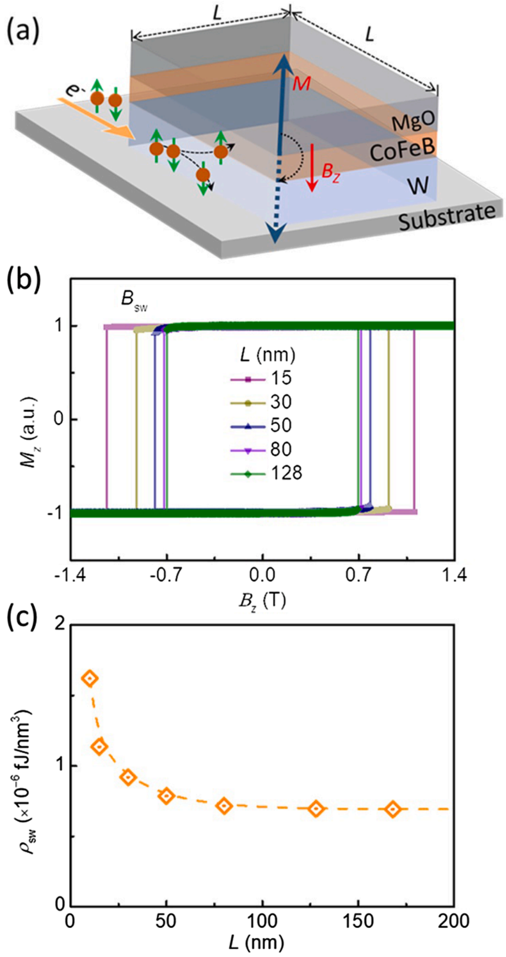

Table 1: Simulation parameters

Parameters	Values used in this work
Saturation magnetization M_s	1 MA/m
Exchange constant A	15 pJ/m
Magnetic anisotropy energy K_u	1 MJ/m^3
Damping constant α	0.012
Dzyaloshinskii-Moriya interaction (DMI) constant	–0.73 mJ/m^2
Spin Hall angle θ_{SHA}	0.3
Anisotropy field H_k	0.75 T
Domain wall width δ_{DW}	15 nm
CoFeB nanosquare size (Length × Width × Thickness)	L nm × L nm × 1 nm
Simulation cell size (Length × Width × Thickness)	1 nm × 1 nm × 1 nm

Fig. 1. (a) Schematic of W/CoFeB/MgO stack under investigation. (b) The magnetic hysteresis loops of CoFeB nanosquares with the variable square side length *L*. (c) The switching energy density of various CoFeB nanosquare sizes. Table 1 summarizes the material parameters used in this study.

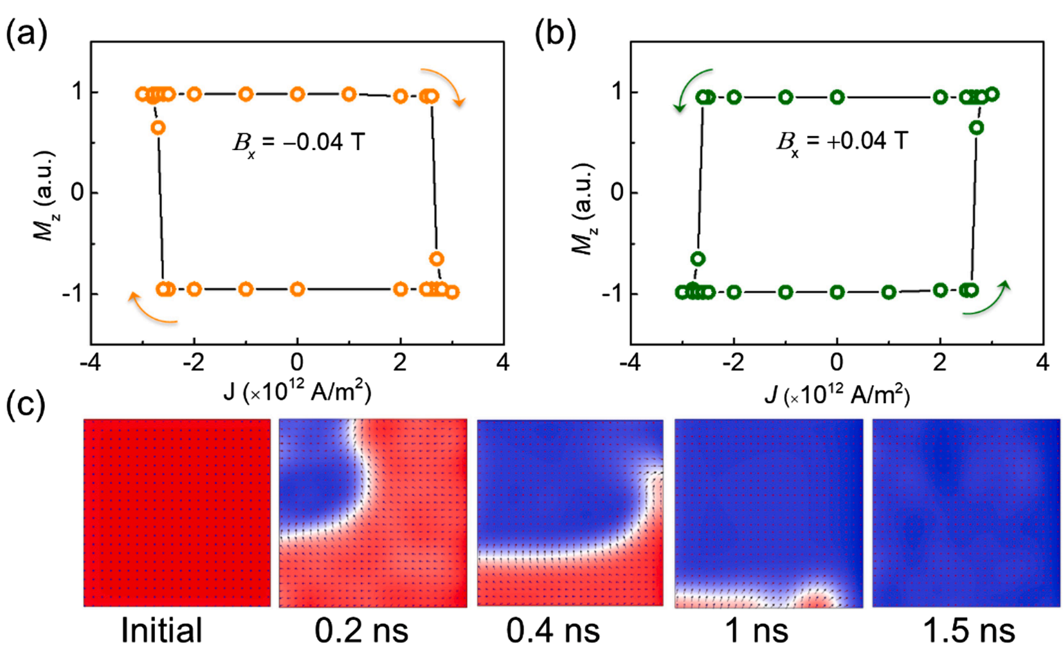

Fig. 2. (a) and (b) The switching loops induced by single current pulses under an in-plane field of $B_x = 0.04$ T and $B_x = 0.04$ T, respectively. (c) The snapshot of the reversal process of CoFeB nanosquare from up-domain to down-domain. The colours red, white, and blue represents up, in-plane, and down magnetization, respectively.

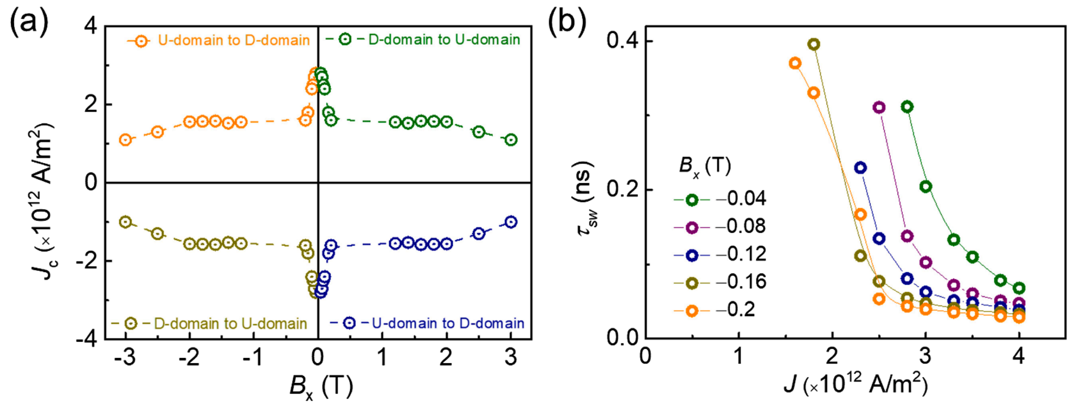

Fig. 3. (a) Critical switching current density J_c under in-plane magnetic field B_x, for all four permutations of domain direction and B_x. (b) The switching time τ_{sw} with the injection current density, under various B_x.

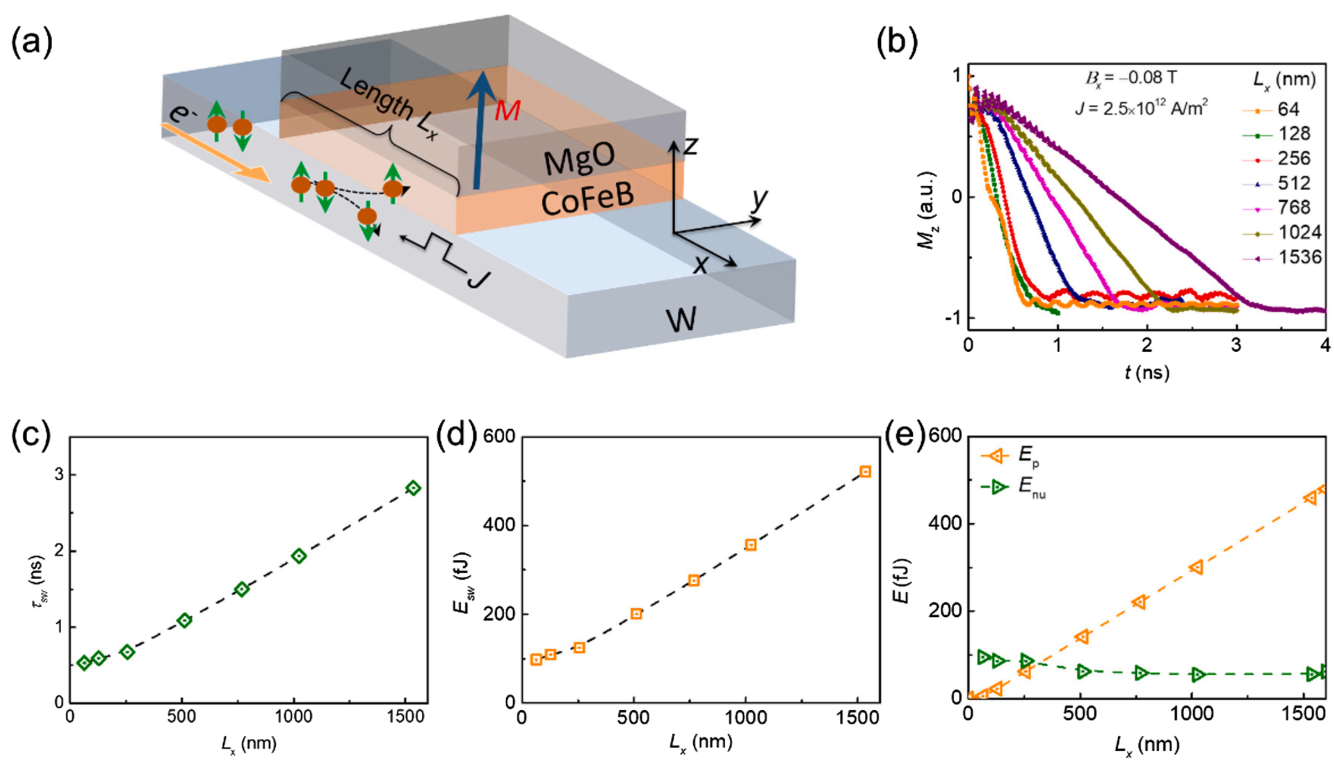

Fig. 4. (a) Schematic of the simulated CoFeB nanowire devices with variable length L_x. (b) The magnetization evolution with the simulation time of devices with various L_x. (c) and (d) The switching time and energy of nanowire with different lengths L_x. (e) DW propagation energy E_p and nucleation energy E_{nu} with CoFeB nanowire length L_x.

magnetization M_s is 1 MA/m, the exchange constant A is 15 pJ/m, the magnetic anisotropy energy K_u is 1 MJ/m^3, the damping constant α is 0.012, DMI value is −0.73 mJ/m^2, the spin Hall angle θ_{SHA} is 0.3. The anisotropy field H_k is 0.75 T, calculated from $H_k = 2K_u/M_s - \mu_0 M_s$, and the domain wall width δ_{DW} is around 15 nm, derived from $\delta_{DW} = \pi\sqrt{A/K_u}$ [36]. The thin ferromagnetic CoFeB nanosquare is defined with a variable square side length L and a fixed thickness of 1 nm. The simulation cell size utilized in this work is 1 nm × 1 nm × 1 nm. The material parameters are summarized in Table 1. The magnetization dynamics was resolved by using the Landau-Lifshitz-Gilbert (LLG) equation that includes SOT, expressed as Eq. (1),

$$\frac{\partial \boldsymbol{M}}{\partial t} = \frac{\gamma}{1+\alpha^2}\left(\boldsymbol{M}\times\boldsymbol{B}_{eff}\right) + \frac{\gamma\alpha}{1+\alpha^2}\left(\boldsymbol{M}\times\left(\boldsymbol{M}\times\boldsymbol{B}_{eff}\right)\right) + \tau_{SOT} \quad (1)$$

Here, γ is the gyromagnetic ratio, $\boldsymbol{M}$ is the magnetization, $\boldsymbol{B}_{\mathbf{eff}}$ is the effective magnetic field, and τ_{SOT} is the spin–orbit torque. τ_{SOT} can be written as Eq. (2),

$$\tau_{SOT} = a_{DL}(\boldsymbol{M}\times(\boldsymbol{p}\times\boldsymbol{M})) - b_{FL}(\boldsymbol{M}\times\boldsymbol{p}) \quad (2)$$

Where $\boldsymbol{P}$ is the spin polarization direction, a_{DL} is the efficiency of damping-like torque and b_{FL} is the efficiency of field-like torque.

3. Results and discussions

First, we investigated magnetic field-driven magnetization switching by applying an external magnetic field B_z along the out-of-plane direction for CoFeB nanosquares with different L, to identify the difference in switching energy with device size. Their major hysteresis loops are presented in Fig. 1(b). The switching field B_{sw} decreased from 1.6 to 0.7 T with increasing L from 15 to 128 nm. The reduction in B_{sw} arises from

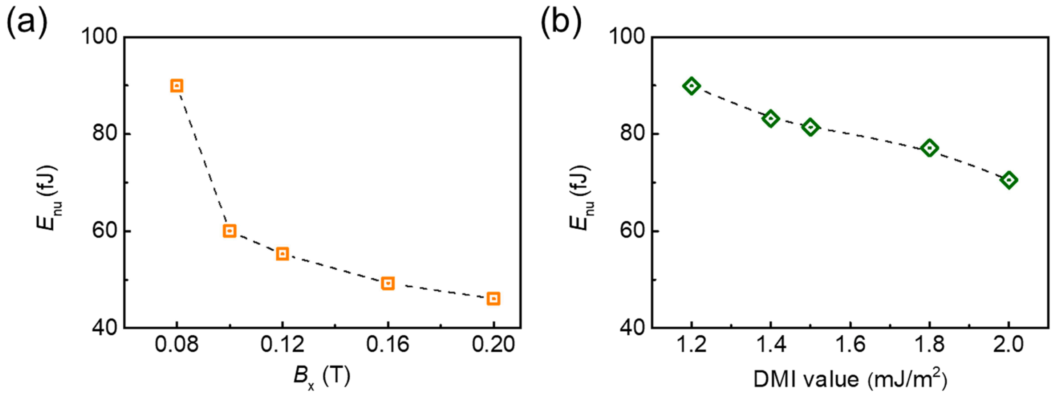

Fig. 5. The nucleation energy under (a) in-plane fields and (b) DMI values.

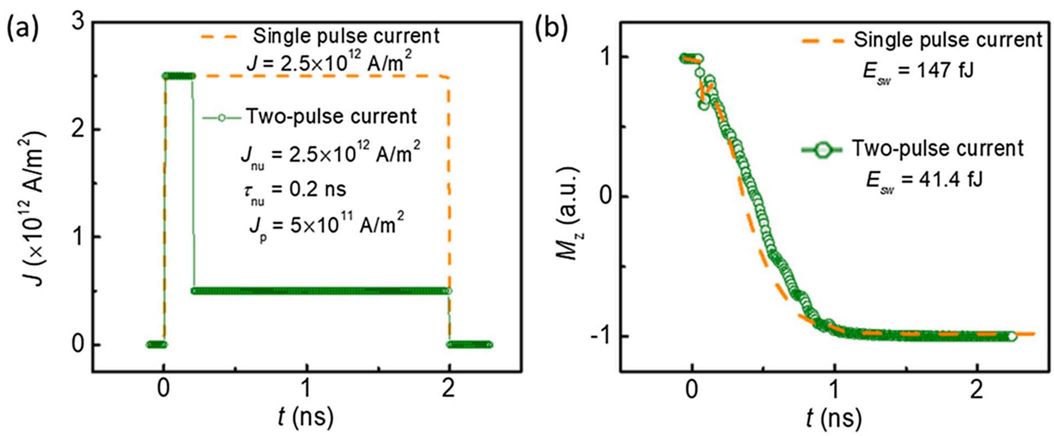

Fig. 6. (a) Schematic of single pulse current and two-pulse current. (b) Comparison of magnetization evolution driven by single pulse current and two-pulse current.

the transition in the switching mechanism from coherent switching as a single domain into multi-domain nucleation and propagation at larger L [37]. The average switching energy density ρ_{sw} calculated from $\rho_{sw} = B_{SW}M_s$, are plotted in Fig. 1(c) as a function of L. The two regimes with rapidly decreasing and asymptotic ρ_{sw} with L represents the single and multi-domain switching, respectively. Thus, a representative maximal single domain size that can be initially nucleated during switching, lies at the transition of these two regimes, at approximately 50–60 nm. In the following discussions, we consider the single domain size as 55 nm, which is consistent with the experimentally reported CoFeB films [38,39,40]. In general, the lateral dimension of the previously reported MTJs of SOT-MRAM was approximately 100 nm, corresponding to the multi-domain mechanism during magnetization switching [41]. Thus, multi-domain magnetization switching remains technologically relevant.

Next, we focussed on SOT-driven magnetization switching in a CoFeB nanosquare with a lateral size of 128 nm × 128 nm. Fig. 2(a) and 2(b) demonstrate the magnetization switching induced by the single current pulse sweep under an in-plane field $B_x = -0.04$ T and $B_x = +0.04$ T, respectively. Here, B_x was applied to not only achieve deterministic switching, but also set the switching loop's polarity. The snapshot of the switching process from "up" to "down" by injecting a current pulse with a current density $J = 2.8 \times 10^{12}$ A/m^2 is presented in Fig. 2(c). It revealed the switching process based on multi-domain model [19]. Domain nucleation is initiated from the top left corner of the device, followed by current-driven DW propagation across the rest of the device.

For SOT-induced magnetization switching, a model for the critical current density J_c for coherent switching in single-domain was proposed by K. S. Lee *et al.* as $J_c = \frac{2e}{\hbar}\frac{M_s t_F}{\theta_{SH}}\left(\frac{H_k}{2} - \frac{B_x}{\sqrt{2}}\right)$ [42]. Based on the single-domain model, the J_c can be estimated from H_k and B_x for a practical system with the magnetic layer thickness of t_F and the charge to spin conversion efficiency of θ_{SH}. Fig. 3(a) and 3(b) show the variation of J_c due to varying B_x and switching time τ_{sw} with the injection current density J. Under increasing B_x, J_c is reduced due to B_x inducing magnetization tilting, and lowering the switching energy barrier. τ_{sw} was quantified by considering the duration taken for 96 % switching, where the normalized magnetization changes from + 1 to −0.96. τ_{sw} decreased with increasing current density applied, but current densities beyond 3.5×10^{12} A/m^2 showed significantly diminished benefits in τ_{sw} reduction because τ_{sw} became dominated by the time spent nucleating the initial reversed domain. The existing model established by K. S. Lee *et al.* offers general relations between the parameters discussed above but is not directly applicable to our regime of interest where switching occurs via domain nucleation and propagation. In general, J required for domain depinning is much lower than that for domain nucleation. The main energy consumption for current-induced magnetization reversal is used to nucleate a reversed domain. In order to estimate the total energy for domain nucleation and propagation, we perform the micro-spin simulation. We take the assumption of the switching energy E_{sw} for a nanowire as the summation of the domain nucleation energy E_{nu} and DW propagation/depinning energy E_p, $E_{sw} = E_{nu} + E_p$. For nanowires with increasing length but constant width, E_p scales linearly with the nanowire area and length. On the other hand, E_{nu} is taken as a constant, independent of nanowire length that are much longer than the initial reversed domain size. By considering a constant DW velocity, then $E_{sw} = (Jwt)^2R\tau_{sw} = E_{nu} + (J_pwt)^2R\tau_p$. Here, w, t, and R represent the width, thickness, and resistance of the nanowire, respectively. J_p and τ_p are the propagation current density and propagation time for complete switching.

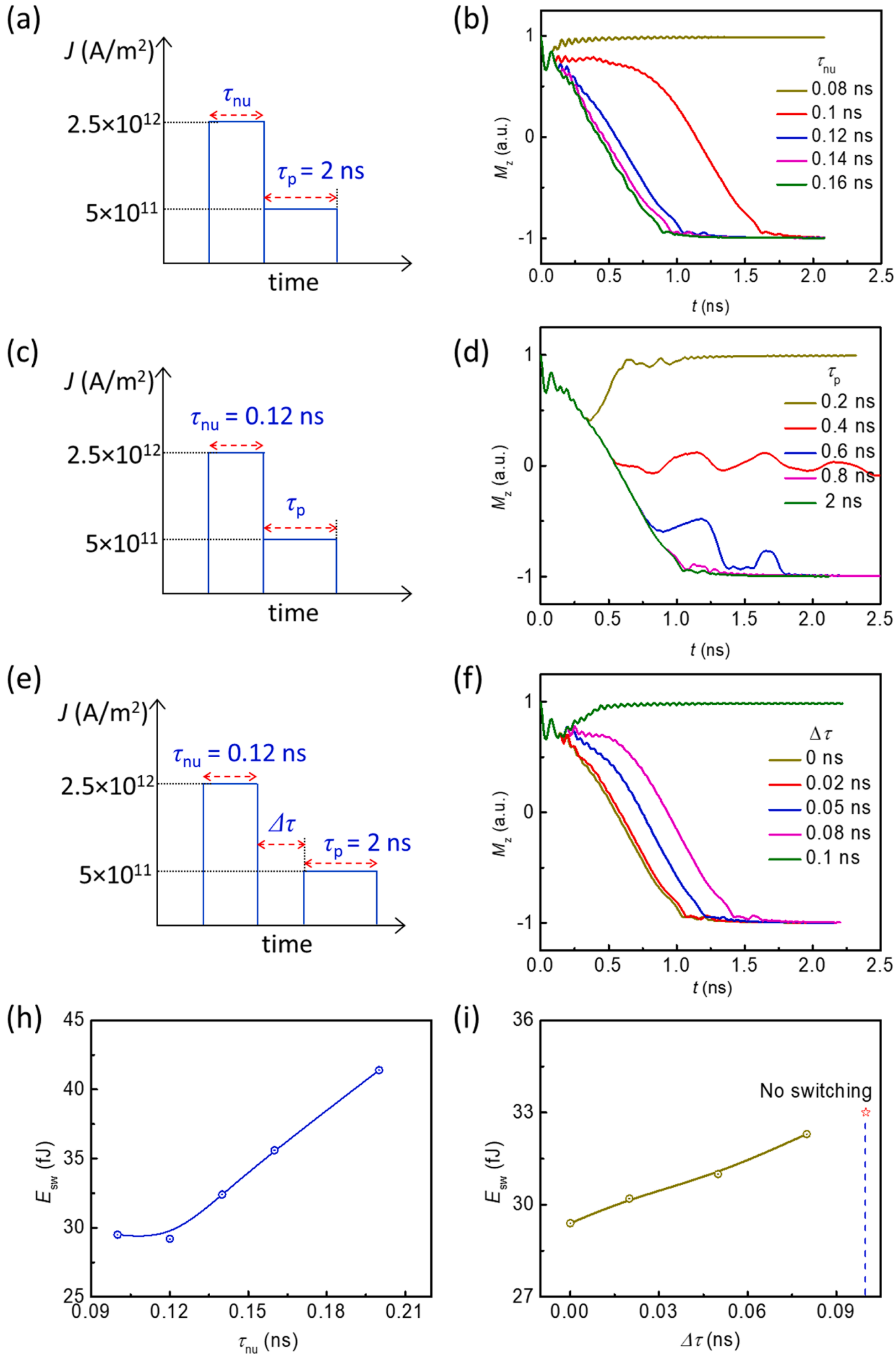

Fig. 7. Schematic of two-pulse current with various (a) τ_{nu}, (c) τ_p, and (e) $\Delta\tau$. (b), (d) and (f) magnetization evolution with simulation time t. Switching energy by varying (h) τ_{nu} and (i) $\Delta\tau$.

Fig. 4(a) shows the simulated CoFeB system with various nanowire lengths L_x and a fixed nanowire width of 128 nm. Fig. 4(b) shows the magnetization evolution over time for L_x from 64 to 1536 nm under $J = 2.5 \times 10^{12}$ A/m^2, and B_x = -0.08 T. The change in τ_{sw} and E_{sw} with L_x are plotted in Fig. 4(c) and 4(d), respectively. Both τ_{sw} and E_{sw} increased linearly with L_x for L_x above 100 nm, as the DWs underwent identical propagation behaviour after the initial domain nucleation. However, when L_x was approximately 64 nm, τ_{sw} and E_{sw} remained relatively unchanged. This was due to the nanowire size approaching the single domain limit, and the reversal process became dominated by the coherent switching.

To resolve E_p and E_{nu} from the overall E_{sw}, the slope of the linear increasing E_{sw} with L_x provides the E_p per unit length. By considering the initial reversed domain size of 55 nm, E_p can be derived by assuming the remaining segment of the wire switched via DW propagation. Thus, $E_p =$ (E_p per unit length) $\times$ (L_x–initial reversed domain size) can be calculated, and the excess energy was attributed to E_{nu}. Fig. 4(e) plots the derived E_p and E_{nu} against L_x, where E_p increased linearly while E_{nu} approached a constant of 56 fJ for large L_x. However, for the range of L_x below 100 nm, E_{nu} was slightly raised up to 88 fJ, being almost five times higher than E_p. Such high E_{nu} limits high-energy efficiency SOT devices.

To gain insights into the reduction of E_{nu}, we performed the simulation study of tuning B_x and DMI strength. Fig. 5(a) and 5(b) show the E_{nu} with B_x and DMI values, respectively. When B_x increases from 0.08 T to 0.2 T, E_{nu} reduces from 90 fJ to 45 fJ. While B_x is effective in reducing E_{nu}, its practical application is limited because B_x beyond 0.2 T would require an external energy supply. The tuning of DMI strength is more applicable for practical applications. DMI reduces E_{nu}, as demonstrated in Fig. 5(b), due to the increasing in-plane magnetization component induced, leading to reduced switching energy potential [43,44,45].

To further improve the energy efficiency, in the next study, we propose the two-pulse current switching scheme where two different current densities are used to optimize energy use for domain nucleation and the subsequent DW propagation. The simulated CoFeB device has the dimensions of 128 nm $\times$ 128 nm $\times$ 1 nm with a B_x of 0.08 mT applied for deterministic switching. Fig. 6 shows the E_{sw} comparison between a single-pulse and two-pulse switching scheme. For the single pulse switching scheme performed using a constant current density of 2.5×10^{12} A/m^2, magnetization switching occurred at 0.72 ns. Taking $\tau_{sw} =$ 0.72 ns, E_{sw} is calculated to be 147 fJ. For the two-pulse switching scheme, a nucleation current with a density of 2.5×10^{12} A/m^2 and a duration of 0.2 ns was first injected, followed by the weaker propagation current with a density of 5×10^{11} A/m^2 to complete the switching process. E_{sw} is reduced significantly to 41.4 fJ with a τ_{sw} of 0.82 ns. This E_{sw} reduction is due to the use of a lower driving current for DW propagation. E_p is proportional to $J_p{}^2 t_p$, to just be linearly proportional with J_p.

Additional simulations have been performed to identify the influence of pulse width and interval $\Delta\tau$ on the two-pulse current scheme, as presented in Fig. 7(a-f). Fig. 7(h) and 7(i) summarize E_{sw} with various τ_{nu} and $\Delta\tau$. Fig. 7(a) shows the illustration of the nucleation pulse width τ_{nu} on switching with a fixed propagation pulse width τ_p of 2 ns and zero pulse interval $\Delta\tau$. τ_p of 2 ns is excessive and used to ensure full switching. Fig. 7(b) shows a clear minimum τ_{nu} required to achieve full switching, and a switching time that decreases and saturates rapidly with increasing τ_{nu}. The switching energy E_{sw} barely increased at $\tau_{nu} = 0.12$ ns, as shown in Fig. 7(h). It demonstrates the significant decrease in switching time can be obtained without a trade-off in E_{sw} within this τ_{nu} range. Fig. 7(c) shows the illustration of the influence of τ_p on switching using a fixed $\tau_{nu} = 0.12$ ns and $\Delta\tau = 0$ ns. Here, the relationship is straightforward where the minimum τ_p required to achieve full switching is optimal. Fig. 7(d) shows the increasing degree of switching with increasing τ_p and the switching process converging towards that at $\tau_p = 2$ ns. Under insufficient τ_p, an oscillatory behavior in perpendicular magnetization M_z is observed, and corresponds to the back hopping of the DW occurring due to DW reflection effect [46]. Fig. 7(e) shows the illustration of the influence of $\Delta\tau$ on switching with a fixed $\tau_{nu} = 0.12$ ns and $\tau_p = 2$ ns. A maximum threshold $\Delta\tau = 0.10$ ns, above which no full switching is achieved and a decreasing switching time below this threshold, as determined in Fig. 7(f). Additionally, Fig. 7(i) shows a linear trend in E_{sw} with $\Delta\tau$, highlighting that the $\Delta\tau$ should be minimized for not only switching time but also E_{sw}. For an optimal switching process using the two-pulse current scheme balancing the switching time and energy, τ_{nu}, τ_p and $\Delta\tau$ generally should be minimized to the point where full switching remains achievable. However, for τ_{nu}, a small regime where E_{sw} barely increases while switching time reduces significantly with increasing τ_{nu} can be exploited.

4. Conclusion

We systematically studied SOT-induced magnetization switching energy by analyzing the constituent domain nucleation and DW propagation processes. The use of in-plane magnetic field and DMI were demonstrated as effective means of lowering nucleation energy. Furthermore, the two-pulse current writing scheme with a lowered current density applied for DW propagation was verified to significantly reduce the switching energy, without tradeoff in switching time. This work, herein, establishes the approaches for the quantification and optimization of high-energy efficiency SOT-MRAM applications.

Declaration of Competing Interest

The authors declare that they have no known competing financial interests or personal relationships that could have appeared to influence the work reported in this paper.

Data availability

Data will be made available on request.

Acknowledgments

The work was supported by the National Research Foundation of Singapore (CRP grant NRF-CRP21-2018-0003). The work was also supported by RIE2020 AME IAF-ICP Grant (I1801E0030). The support from National Natural Science Foundation of China (NSFC-12064024) is also acknowledged.

References

[1] K. Galatsis, C. Ahn, I. Krivorotov, P. Kim, R. Lake, K.L. Wang, J.P. Chang, A material framework for beyond-CMOS devices, IEEE Circuits Syst. Mag. 1 (2015) 19–27.
[2] J.-Q. Yang, Y.e. Zhou, S.-T. Han, Functional applications of future data storage devices, Adv. Electron. Mater. 7 (5) (2021) 2001181.
[3] S. Bhatti, R. Sbiaa, A. Hirohata, H. Ohno, S. Fukami, S.N. Piramanayagam, Spintronics based random access memory: a review, Mater. Today 20 (9) (2017) 530–548.
[4] T. Suzuki, H. Tanigawa, Y. Kobayashi, K. Mori, Y. Ito, Y. Ozaki, K. Suemitsu, T. Kitamura, K. Nagahara, E. Kariyada, N. Ohshima, S. Fukami, M. Yamanouchi, S. Ikeda, M. Hayashi, M. Sakao, H. Ohno, Low-current domain wall motion MRAM with perpendicularly magnetized CoFeB/MgO magnetic tunnel junction and underlying hard magnets. 2013 Symposium on VLSI Technology, 2013.
[5] Z. Guo, J. Yin, Y. Bai, D. Zhu, K. Shi, G. Wang, K. Cao, W. Zhao, Spintronics for energy-efficient computing: An overview and outlook, Proc. IEEE. 109 (2021) 1398–1417.
[6] R. Sbiaa, S.N. Piramanayagam, Recent developments in spin transfer torque MRAM, Phys. Status Solidi - Rapid Res. Lett. 11 (2017) 1700163.
[7] L. Liu, C.-F. Pai, Y. Li, H.W. Tseng, D.C. Ralph, R.A. Buhrman, Spin-torque switching with the giant spin Hall effect of tantalum, Science 336 (6081) (2012) 555–558.
[8] J.C. Slonczewski, Current-driven excitation of magnetic multilayers, J. Magn. Magn. Mater. 159 (1-2) (1996) L1–L7.
[9] W. Kong, C. Wan, C. Guo, C. Fang, B. Tao, X. Wang, X. Han, All-electrical manipulation of magnetization in magnetic tunnel junction via spin–orbit torque, Appl. Phys. Lett. 116 (2020) 162401.
[10] C.W. Cheng, C. Shiue, T.I. Cheng, G. Chern, Observation of parallel-antiparallel magnetic coupling in ultrathin CoFeB-MgO based structures with perpendicular magnetic anisotropy, J. Appl. Phys. 112 (2012) 033917.
[11] J. H. Lim, N. Raghavan, A. Padovani, J. H. Kwon, K. Yamane, H. Yang, V. B. Naik, L. Larcher, K. H. Lee, K. L. Pey, Investigating the statistical-physical nature of MgO dielectric breakdown in STT-MRAM at different operating conditions, 2018 IEEE International Electron Devices Meeting (IEDM).
[12] W. Zhao, X. Zhao, B. Zhang, K. Cao, L. Wang, W. Kang, Q. Shi, M. Wang, Y. u. Zhang, Y. Wang, S. Peng, J.-O. Klein, L. de Barros Naviner, D. Ravelosona, Failure analysis in magnetic tunnel junction nanopillar with interfacial perpendicular magnetic anisotropy, Materials 9 (1) (2016) 41.

[13] L. Liu, T. Moriyama, D.C. Ralph, R.A. Buhrman, Spin-Torque Ferromagnetic Resonance Induced by the Spin Hall Effect, Phys. Rev. Lett. 106 (2011), 036601.
[14] S. Fukami, T. Anekawa, C. Zhang, H. Ohno, A spin–orbit torque switching scheme with collinear magnetic easy axis and current configuration, Nat. Nanotechnol. 11 (7) (2016) 621–625.
[15] C.F. Pai, Y. Ou, L.H. Vilela-Leão, D. Ralph, R. Buhrman, Dependence of the efficiency of spin Hall torque on the transparency of Pt/ferromagnetic layer interfaces, Phys. Rev. B 92 (2015), 064426.
[16] C. Zhang, S. Fukami, K. Watanabe, A. Ohkawara, S. Dutta Gupta, H. Sato, F. Matsukura, H. Ohno, Critical role of W deposition condition on spin-orbit torque induced magnetization switching in nanoscale W/CoFeB/MgO, Appl. Phys. Lett. 109 (2016) 192405.
[17] F. Luo, S. Goolaup, W.C. Law, S. Li, F. Tan, C. Engel, T. Zhou, W.S. Lew, Quantification of spin accumulation causing spin-orbit torque in Pt/Co/Ta stack, Phys. Rev. B 95 (2017), 174415.
[18] M. Yang, Y. Deng, K. Cai, H. Ju, S. Liu, B. Li, K. Wang, Deterministic magnetic switching of perpendicular magnets by gradient current density, J. Magn. Magn. Mater. 489 (2019) 165474.
[19] X. Zhao, L. Ji, W. Liu, S. Li, L. Liu, Y. Song, Y. Li, J. Ma, X. Sun, H. Wang, X. Zhao, Z. Zhang, Field-free switching of a spin-orbit-torque device through interlayer-coupling-induced domain walls, Phys. Rev. Appl. 13 (4) (2020), 044074.
[20] J. Cao, Y. Chen, T. Jin, W. Gan, Y. Wang, Y. Zheng, H. Lv, S. Cardoso, D. Wei, W. S. Lew, Spin orbit torques induced magnetization reversal through asymmetric domain wall propagation in Ta/CoFeB/MgO structures, Sci. Rep. 8 (2018) 1355.
[21] N. Murray, W.B. Liao, T.C. Wang, L.J. Chang, L.Z. Tsai, T.Y. Tsai, S.F. Lee, C.F. Pai, Field-free spin-orbit torque switching through domain wall motion, Phys. Rev. B 100 (2019), 104441.
[22] X. Zhao, Y. Liu, D. Zhu, M. Sall, X. Zhang, H. Ma, J. Langer, B. Ocker, S. Jaiswal, G. Jakob, M. Kläui, Spin–orbit torque driven multi-level switching in He+ irradiated W/CoFeB/MgO Hall bars with perpendicular anisotropy, Appl. Phys. Lett. 116 (2020), 242401.
[23] M. Wang, W. Cai, D. Zhu, Z. Wang, J. Kan, Z. Zhao, K. Cao, Z. Wang, Y. Zhang, T. Zhang, C. Park, J.-P. Wang, A. Fert, W. Zhao, Field-free switching of a perpendicular magnetic tunnel junction through the interplay of spin–orbit and spin-transfer torques, Nat. Electron. 1 (11) (2018) 582–588.
[24] W. Cai, K. Shi, Y. Zhuo, D. Zhu, Y. Huang, J. Yin, K. Cao, Z. Wang, Z. Guo, Z. Wang, G. Wang, Sub-ns field-free switching in perpendicular magnetic tunnel junctions by the interplay of spin transfer and orbit torques, IEEE Electron Device Lett. 42 (2021) 704–707.
[25] S.S. Parkin, M. Hayashi, L. Thomas, Magnetic domain-wall racetrack memory, Science 320 (5873) (2008) 190–194.
[26] E. Raymenants, O. Bultynck, D. Wan, T. Devolder, K. Garello, L. Souriau, A. Thiam, D. Tsvetanova, Y. Canvel, D.E. Nikonov, I.A. Young, Nanoscale domain wall devices with magnetic tunnel junction read and write, Nat. Electron. 4 (2021) 392–398.
[27] Z. Luo, A. Hrabec, T.P. Dao, G. Sala, S. Finizio, J. Feng, S. Mayr, J. Raabe, P. Gambardella, L.J. Heyderman, Current-driven magnetic domain-wall logic, Nature 579 (2020) 214–218.
[28] C.H. Wan, M.E. Stebliy, X. Wang, G.Q. Yu, X.F. Han, A.G. Kolesnikov, M.A. Bazrov, M.E. Letushev, A.V. Ognev, A.S. Samardak, Gradual magnetization switching via domain nucleation driven by spin–orbit torque, Appl. Phys. Lett. 118 (2021) 032407.
[29] D. Kumar, T. Jin, R. Sbiaa, M. Kläui, S. Bedanta, S. Fukami, D. Ravelosona, S. H. Yang, X. Liu, S.N. Piramanayagam, Domain wall memory: Physics, materials, and devices, Phys. Rep. 958 (2022) 1–35.
[30] A. Vansteenkiste, J. Leliaert, M. Dvornik, M. Helsen, F. Garcia-Sanchez, B. Van Waeyenberge, The design and verification of MuMax3, AIP Adv. 4 (2014) 107133.
[31] C.F. Pai, L. Liu, Y. Li, H. Tseng, D. Ralph, R. Buhrman, Spin transfer torque devices utilizing the giant spin Hall effect of tungsten, Appl. Phy. Lett. 101 (2012) 122404.
[32] J. Kim, J. Sinha, M. Hayashi, M. Yamanouchi, S. Fukami, T. Suzuki, S. Mitani, H. Ohno, Layer thickness dependence of the current-induced effective field vector in Ta/CoFeB/MgO, Nat. Mater. 12 (2013) 240–245.
[33] S. Cho, S.C. Baek, K.D. Lee, Y. Jo, B.G. Park, Large spin Hall magnetoresistance and its correlation to the spin-orbit torque in W/CoFeB/MgO structures, Sci. Rep. 5 (2015) 14668.
[34] Y. Takeuchi, C. Zhang, A. Okada, H. Sato, S. Fukami, H. Ohno, Spin-orbit torques in high-resistivity-W/CoFeB/MgO, Appl. Phys. Lett. 112 (2018) 192408.
[35] D.M. Lattery, D. Zhang, J. Zhu, X. Hang, J.-P. Wang, X. Wang, Low Gilbert damping constant in perpendicularly magnetized W/CoFeB/MgO films with high thermal stability, Sci. Rep. 8 (2018) 1.
[36] B. Dieny, M. Chshiev, Perpendicular magnetic anisotropy at transition metal/oxide interfaces and applications, Rev. Mod. Phys. 89 (2017), 025008.
[37] J.M. Coey, Magnetism and magnetic materials, Cambridge University Press, 2010.
[38] C. Zhang, S. Fukami, H. Sato, F. Matsukura, H. Ohno, Spin-orbit torque induced magnetization switching in nano-scale Ta/CoFeB/MgO, Appl. Phys. Lett. 107 (2015) 012401.
[39] H. Lv, J. Fidalgo, A.V. Silva, D.C. Leitao, T. Kampfe, J. Langer, J. Wrona, B. Ocker, P.P. Freitas, S. Cardoso, Multi-Level Switching and reversible current driven domain-wall motion in single CoFeB/MgO/CoFeB-based perpendicular magnetic tunnel junctions, Adv. Electron. Mater. 7 (2) (2021) 2000976.
[40] C.-W. Chien, D.-Y. Wang, S.-H. Huang, K.-H. Shen, S.-Y. Yang, J.-H. Shyu, C.-Y. Lo, K.-M. Kuo, Y.-S. Chen, Y.-H. Wang, T.-K. Ku, D.-L. Deng, Scaling properties of step-etch perpendicular magnetic tunnel junction with dual-CoFeB/MgO interfaces, IEEE Electron Device Lett. 35 (7) (2014) 738–740.
[41] K. Garello, F. Yasin, H. Hody, S. Couet, L. Souriau, S. H. Sharifi, J. Swerts, R. Carpenter, S. Rao, W. Kim, J. Wu, K. K. V. Sethu, M. Pak, N. Jossart, D. Crotti, A. Furnémont, G. S. Kar, Manufacturable 300mm platform solution for field-free switching SOT-MRAM, 2019 Symposium on VLSI Circuits, T194-T195 (2019).
[42] K.S. Lee, S.W. Lee, B.C. Min, K.J. Lee, Threshold current for switching of a perpendicular magnetic layer induced by spin Hall effect, Appl. Phys. Lett. 102 (2013) 112410.
[43] L.H. Diez, M. Voto, A. Casiraghi, M. Belmeguenai, Y. Roussigné, G. Durin, A. Lamperti, R. Mantovan, V. Sluka, V. Jeudy, Y.T. Liu, A. Stashkevich, S.M. Chérif, J. Langer, B. Ocker, L. Lopez-Diaz, D. Ravelosona, Enhancement of the Dzyaloshinskii-Moriya interaction and domain wall velocity through interface intermixing in Ta/CoFeB/MgO, Phys. Rev. B 99 (5) (2019), 054431.
[44] C. Garg, S.H. Yang, L. Thompson, T. Topuria, A. Capua, B. Hughes, T. Phung, P. C. Filippou, S.S. Parkin, Efficient chiral-domain-wall motion driven by spin-orbit torque in metastable platinum films, Phys. Rev. Appl. 14 (2020), 034052.
[45] K. Shahbazi, J.-V. Kim, H.T. Nembach, J.M. Shaw, A. Bischof, M.D. Rossell, V. Jeudy, T.A. Moore, C.H. Marrows, Domain-wall motion and interfacial Dzyaloshinskii-Moriya interactions in Pt/Co/Ir(t_{Ir})/Ta multilayers, Phys. Rev. B 99 (2019), 094409.
[46] J. Yoon, S.W. Lee, J.H. Kwon, J.M. Lee, J. Son, X. Qiu, K.J. Lee, H. Yang, Anomalous spin-orbit torque switching due to field-like torque–assisted domain wall reflection, Sci. Adv. 3 (2017), e1603099.

Tianli Jin[a,1], Calvin Ang[a,1], Xuan Wang[b], Wen Siang Lew[a,*], S. N. Piramanayagam[a,*]

[a] *School of Physical and Mathematical Sciences, Nanyang Technological University, Singapore 637371, Singapore*

[b] *School of Science, Lanzhou University of Technology, Lanzhou 730050, China*

[*] Corresponding authors.

E-mail addresses: wensiang@ntu.edu.sg (W. Siang Lew), prem@ntu.edu.sg (S.N. Piramanayagam).

[1] T. Jin and C. Ang contributed equally to this work.